Dalton Transactions

ROYAL SOCIETY OF CHEMISTRY

PAPER

View Article Online
View Journal | View Issue

Cite this: *Dalton Trans.*, 2024, **53**, 18662

Determination of the high-pressure domain of stability of $BeSiO_3$ and characterization of its crystal structure and properties

Tarik Ouahrani, *[a,b,c] Ruth Franco,[d] Álvaro Lobato,[e] Fernando Izquierdo-Ruiz,[e] Alfonso Muñoz[f] and Daniel Errandonea *[g]

Using density-functional theory calculations, we determined the pressure domain of stability of beryllium metasilicate, $BeSiO_3$, an elusive compound for which no stable polymorph is known until now. We found that $BeSiO_3$ is stable at pressures above 9 GPa, a condition that makes it accessible with a large-volume press. After considering the cubic, orthorhombic, and hexagonal perovskite structures and the Ilmenite structure, known from related compounds, we propose that the most stable structure among them is the orthorhombic perovskite structure described by space group *Pnma*. The unit-cell parameters of this structure are a = 4.966 Å, b = 7.160 Å, and c = 4.374 Å. We also determined the frequencies of Raman and infrared phonons, the elastic constants and modulus, and the electronic band structure for the orthorhombic perovskite structure. Finally, the pressure dependence of unit-cell parameters was calculated. Compression was found to be slightly anisotropic, with the axial compressibilities decreasing following the sequence $\kappa_b > \kappa_c > \kappa_a$. In addition, we found that $BeSiO_3$ is quite incompressible with a bulk modulus of 242 GPa, which makes it one of the less compressible silicates. To understand, such a large bulk modulus, both the quantum theory of atoms in molecules and the electron localization function decomposition were utilized to analyze the bonding and to relate it to the mechanical properties.

Received 23rd July 2024,
Accepted 17th October 2024

DOI: 10.1039/d4dt02123a

rsc.li/dalton

1. Introduction

The rocks that compose the mantle of the Earth and the rest of terrestrial planets are mostly silicates. Common silicates found in the mantle of our planet include olivine, garnet, and pyroxene, but also zircon and perovskite. In particular, $CaSiO_3$ perovskite is thought to constitute between 6 wt% and 12 wt% of the lower mantle of the Earth.[1] Beryllium orthosilicate, the mineral phenakite (Be_2SiO_4), is also a constituent in the mantle of the Earth. This nesosilicate is found in pegmatite veins and its crystal structure is characterized by the fact that it is formed by isolated SiO_4 tetrahedral units which are not directly connected with mutual oxygen atoms, as in other silicates, but by interstitial cations.[2] It is known that other silicates, in particular metasilicates, can be formed in the $BeO–SiO_2$ system.[3] This group of silicates, because of their structural characteristics, provides an ideal test for various theoretical and empirical models of the behavior of silicates under high pressure (HP) conditions.[4] Metasilicates, like beryl ($Al_2Be_3(SiO_3)_6$), are no so abundant as orthosilicates. However, they are interesting for materials chemistry because they are known to have peculiar structural properties, including non-isotropic thermal expansion and compression.[5] They are also of great interest to various industries because they have a high hardness, good to excellent wear and corrosion resistance, and low cost.[6] In particular, $BeSiO_3$, an analogous metasilicate to $CaSiO_3$, has been reported to exist and it is commercially available from American Elements (Los Angeles, California, USA), being a white crystalline powder. Apparently, $BeSiO_3$ can be prepared by calcining a mixture of beryllium oxide, BeO, with silica, SiO_2, at an elevated temperature.[6] However, $BeSiO_3$ has been a very elusive material and its crystal structure and physical properties remain unknown.

[a]*Ecole sup érieure en sciences appliqu ées, ESSA-Tlemcen, BB 165 RP Bel Horizon, Tlemcen 13000, Algeria. E-mail: tarik_ouahrani@yahoo.fr*
[b]*Laboratoire de Physique Théorique, Université de Tlemcen, BP 119, 13000, Algeria*
[c]*Université de Lorraine, Laboratoire Lorrain de Chimie Mol éculaire, CNRS, L2CM, F-57000 Metz, France*
[d]*Matter at High Pressure (MALTA) Consolider Team and Departamento de Química Física y Analítica, Universidad de Oviedo, E-33006 Oviedo, Spain*
[e]*Matter at High Pressure (MALTA) Consolider Team and Department of Physical Chemistry, University Complutense of Madrid, 28040 Madrid, Spain*
[f]*Departamento de F ísica, MALTA Consolider Team, Universidad de La Laguna, San Crist óbal de La Laguna, Tenerife E-38200, Spain*
[g]*Departamento de Física Aplicada – Instituto de Ciencia de Materiales, Matter at High Pressure (MALTA) Consolider Team, Universidad de Valencia, Edificio de Investigación, C/Dr. Moliner 50, Burjassot, 46100 Valencia, Spain.*
E-mail: daniel.errandonea@uv.es

Density-functional theory (DFT)[7] has become a routine method to predict and understand chemical and physical properties and phase transition. Thus, this technique could be a good strategy to study the stability and properties of $BeSiO_3$, a known material with an unreported crystal structure. Indeed, DFT has been successfully used in the past to study other compounds representing experimental challenges; for instance, $TlVO_4$ [8] and anhydrous $MgSO_4$.[9] To the best of our knowledge, only one DFT study has been performed $BeSiO_3$, according to these simulations, which are presented in the Materials Project,[10] $BeSiO_3$ is proposed to crystallize in a cubic perovskite structure described by space group $Pm\bar{3}m$.[11] This crystal structure is represented using VESTA[12] in Fig. 1a. However, the cubic perovskite structure has been found to be highly unstable because, at ambient conditions, it is energetically most favored the formation of Be_2SiO_4 + SiO_2 than the formation of $BeSiO_3$. A possible avenue to explore in order to synthesize $BeSiO_3$, as a compound that can be stable or metastable at ambient conditions, is the use of high-pressure conditions. The application of high-pressure conditions adds an additional dimension to the chemical phase space, opening up this way an unexplored part of the phase diagram bearing a tremendous potential for contributing to define strategies for the synthesis of novel compounds.[13] Motivated by this fact, we have studied the pressure domain of stability of $BeSiO_3$ a necessary condition for its synthesis in the laboratory.

In this work, we have used DFT calculations to explore the thermodynamic stability of $BeSiO_3$ at 0 K by comparing the enthalpy of four candidate polymorphs and two possible decomposition paths typically observed in different geological processes involving similar metasilicates: Be_2SiO_4 + SiO_2 and BeO + SiO_2. In our computing simulations, we have considered not only the cubic perovskite structure proposed in the Materials Project,[11] but also the orthorhombic perovskite structure described by space group *Pnma*, which has been found to be more stable than the cubic structure in $CaSiO_3$.[14] We have also considered, based on crystal chemistry arguments, like the Bastide diagram,[15] the hexagonal perovskite structure described by space group $P6_3/mmc$[16] and the Ilmenite structure described by space group $R\bar{3}$.[15] These are the kind of structures more commonly observed in perovskite-related compounds. Such an approach has been shown to be successful in the past for making predictions, which were subsequently confirmed by experiments.[8,9] In our study, we have found that the cubic perovskite structure cannot be stabilized in $BeSiO_3$ because it is dynamically unstable. We have also established that the orthorhombic perovskite-type structure is thermodynamically more stable than any of the other phases studied here from 0 to 50 GPa, and more stable than the decomposition products considered in this work at pressures larger than 9 GPa, pressure conditions that can be routinely accessed in the laboratory using a large-volume press[17] and corresponds to about 270 km in depth in the Earth mantle. For the orthorhombic structure, we have also determined several physical properties, including Raman- and infrared (IR)-active phonons, elastic constants and moduli, and the electronic band-gap energy. We have also studied the bonding properties of orthorhombic $BeSiO_3$ and how the crystal structure is modified under compression determining the linear compressibility of each crystallographic axis and a pressure (P)–volume (V) equation of state (EOS). The reported results contrib-

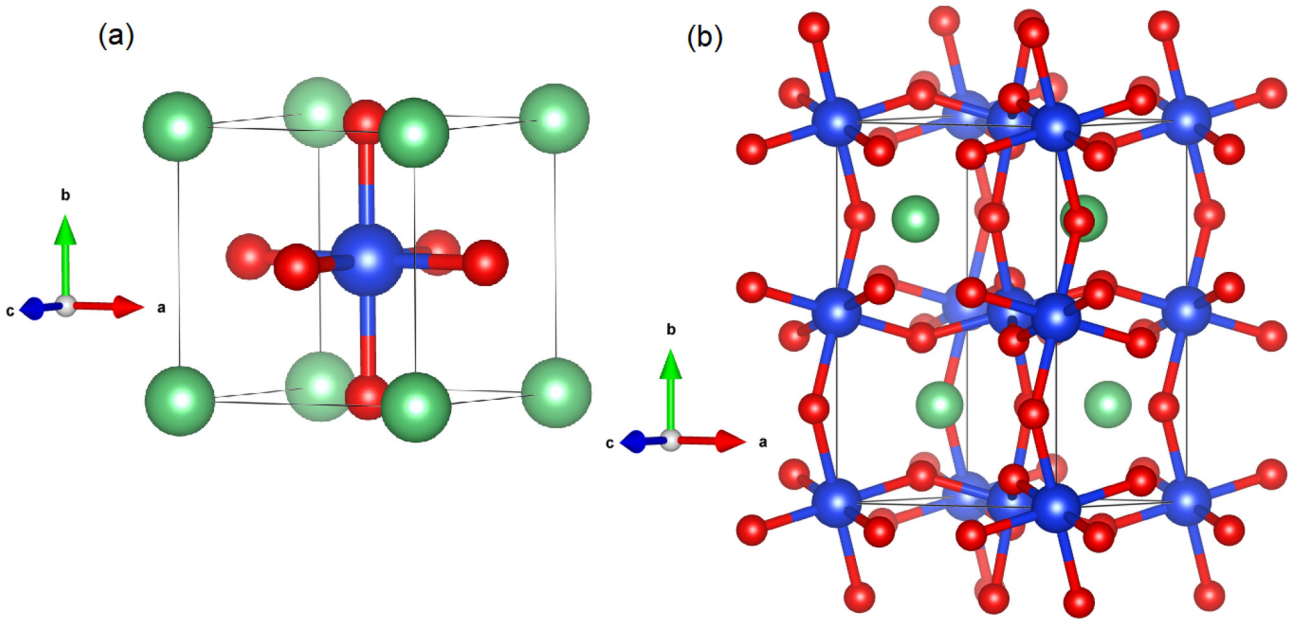

Fig. 1 Crystal structure of the (a) cubic (space group $Pm\bar{3}m$) and (b) orthorhombic (space group *Pnma*) perovskite-type structures of $BeSiO_3$. Beryllium atoms are shown in green, silicon atoms in blue, and oxygen atoms in red. The SiO_6 bonds are drawn in the figures. Crystal structure were drawn with VESTA.[12]

ute to improving the understanding of silicates and their high-pressure behavior.

2. Computational details

Through structural optimization calculations, we have been able to predict the high-pressure structure of $BeSiO_3$ under various pressure conditions. The Vienna *Ab initio* Simulation Package (VASP),[20,21] which performs DFT-based structural calculations, has been employed in the simulations. Several parameters have been carefully monitored to reach the convergence and accuracy of the predicted results. For instance, the threshold of the electronic self-consistent field cycle was adjusted to a value of 10^{-7} eV. Furthermore, convergence tests have led to the establishment of 520 eV as the cutoff energy for plane waves. The traditional Monkhorst–Pack scheme[22,23] has been employed by using in the reciprocal space a dense grid of 12 × 12 × 12 for the cubic perovskite structure, 5 × 4 × 5 for the orthorhombic perovskite structure, 8 × 8 × 4 for the hexagonal perovskite structure, and 8 × 8 × 8 for the Ilmenite structure. In the relaxed equilibrium configuration, the forces were requested to be less than 0.3 meV per Å per atom in each cartesian direction. The electronic band-structure calculations have been simulated using the projector-augmented wave (PAW) method. Using the Perdew–Burke–Ernzerhof (PBE) functional, the exchange–correlation energy has been described within the framework of the generalized-gradient approximation (GGA).[24] Given that the PBE functional typically underestimates the band-gap energy, we have also used the Heyd–Scuseria–Ernzerhof (HSE) hybrid density functional (HSE06)[25] to calculate the band structure as well as the electronic density of state (DOS).

As the VASP code does not include built-in routines for lattice-dynamic calculations, we have conducted such calculations in conjunction with the Phonopy package.[26,27] To check the dynamical properties of the studied compound the force constants and the dynamical matrix have been obtained first using the finite displacement method with VASP on a displaced supercell. We used a 3 × 3 × 3 phonon supercell for cubic system and 3 × 3 × 1 supercell for the orthorhombic one. We have used a Monkhorst–Pack *k*-mesh grid of 3 × 3 × 3 in these calculations. The phonon density of the state (PHDOS) has also been computed on an 11 × 11 × 11 grid. On top of that, we have been able to obtain the assignment of the Raman, Infrared, and Silent modes as well as the reducible representation of the modes at the Γ point of the Brillouin zone with the aid of the Spectral Active Modes (SAM) tool of the Bilbao Crystallographic Server. Using the Critic2 code to calculate the effective charge, we have also investigated the bonding characteristics and the local and polyhedral bulk modulus[28] of the stable structure.[29,30] The algorithm of this code relies on the use of the Quantum Theory of Atoms in Molecules (QTAIM)[31–33] for the topological analysis of scalar functions in the real space. The code provides the nature of interatomic bonds by partitioning the topological space into disjoint regions.[34]

3. Results and discussion

3.1. Structure, stability, and possible synthesis conditions

As mentioned in the introduction, a cubic perovskite structure has been proposed before this study for $BeSiO_3$.[11] This structure is schematically shown in Fig. 1a. In the cubic unit cell, Be atoms are 12-fold coordinated by oxygen atoms and sit in the corners of the cube at the Wyckoff position 1*a* (0, 0, 0) while oxygen atoms are at the face center of the cubic lattice at the Wyckoff position 3*c* (1/2, 1/2, 0), and Si atoms lie within the oxygen octahedral units and occupy the body center at the Wyckoff position 1*b* (1/2, 1/2, 1/2). We have optimized this structure and have found that a = 3.4786 Å at 0 GPa, a value nearly identical to that reported in the Materials Project, 3.477 Å.[11] After the structural optimization, we have calculated the phonon dispersion of the cubic structure, which is plotted in Fig. 2. In the figure, it can be seen that there are several imaginary phonon branches, which means that the cubic perovskite structure is dynamically unstable, excluding the cubic perovskite as a possible structure for $BeSiO_3$.

We have then considered three other crystal structures as candidates for $BeSiO_3$. They are structures related to cubic perovskite, but with a lower symmetry. These structures are commonly observed in ABO_3 compounds.[14–16] As described in the introduction, the candidate structures include the orthorhombic perovskite[14] and the hexagonal perovskite structures,[16] and the Ilmenite[15] structure. As we show in Fig. 3, we found that the orthorhombic perovskite structure, described by space group *Pnma*,[14] is the one with minimum enthalpy between the candidate structures from 0 to 50 GPa, being thus the most stable structure among those here considered. In Fig. 3 it can be seen that, as pressure increases, the enthalpy of the hexagonal perovskite structure approaches that of the orthorhombic perovskite structure, suggesting that at press-

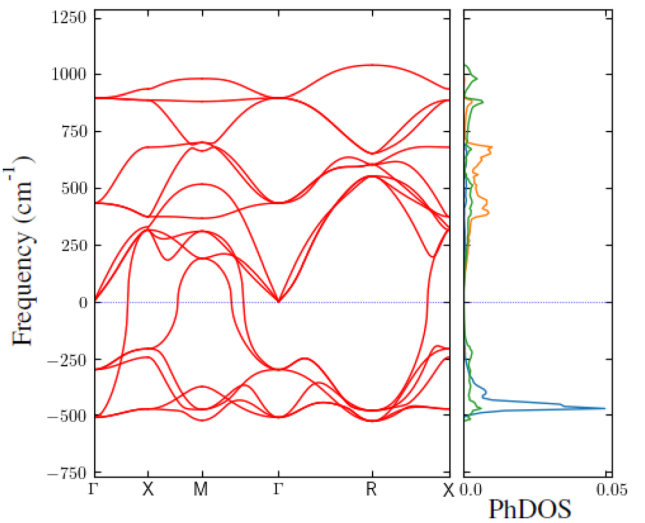

Fig. 2 Phonon dispersion and phonon density of states (PhDOs) of cubic perovskite $BeSiO_3$.

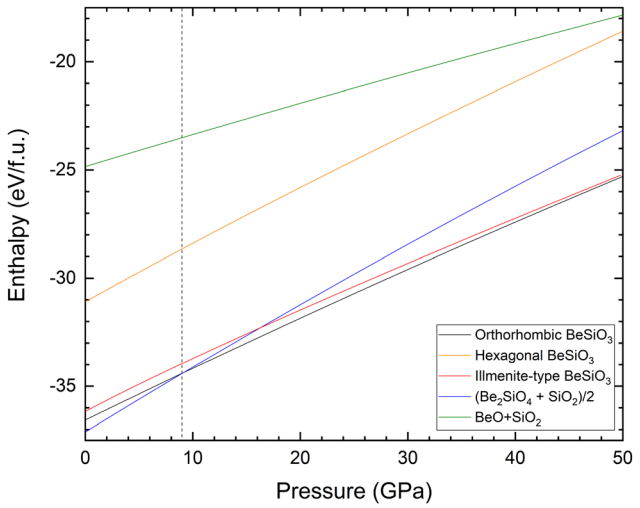

Fig. 3 Enthalpy *versus* pressure of the orthorhombic perovskite, the Ilmenite-type, and the hexagonal perovskite structures of $BeSiO_3$. We also show the enthalpy *versus* pressure of the decomposition paths we have considered $(Be_2SiO_4 + SiO_2)/2$ and $BeO + SiO_2$. The figure shows that orthorhombic $BeSiO_3$ is thermodynamic stable above 9 GPa at 0 K. The vertical dashed line indicates the pressure where the enthalpy of orthorhombic $BeSiO_3$ becomes smaller than that of $(Be_2SiO_4 + SiO_2)/2$.

ures higher than 50 GPa an orthorhombic-hexagonal transition might take place.

We have also found that the orthorhombic perovskite structure does not have imaginary phonon branches at 0 GPa and at elevated pressures up to 50 GPa, being therefore dynamically stable in the pressure range covered by this study. This can be seen in Fig. 4 where we show the phonon dispersion calculated at 0 and 27 GPa. The stabilization of the orthorhombic structure, instead of the cubic structure previously proposed,[11] is consistent with the stability rules of perovskites determined by the Goldschmidt tolerance factor.[18] This factor is an indicator of the stability and distortion of crystal structures. It is defined as

$$t = (r_A + r_O)/(\sqrt{2}(r_B + r_O)) \quad (1)$$

where r_A, r_B, and r_O are the ionic radii of the cations A and B and oxygen. In $BeSiO_3$ this factor is 0.68, which according to Goldschmidt supports the existence of an orthorhombic perovskite structure.[19]

We have also explored the pressure domain of stability of orthorhombic $BeSiO_3$ against a possible chemical decomposition. It has been determined by comparing the enthalpy of orthorhombic $BeSiO_3$ with that of the two most possible decomposition products, as a function of pressure. The results are shown in Fig. 3. At 0 GPa $BeSiO_3$ is slightly unstable against $(Be_2SiO_4 + SiO_2)/2$. On the other hand, the decomposition of $BeSiO_3$ into $BeO + SiO_2$ is not favored at any pressure according to the enthalpy results. On the other hand, we have found that at a pressure of 9 GPa the enthalpy of $BeSiO_3$ becomes smaller than the enthalpy of $(Be_2SiO_4 + SiO_2)/2$. As pressure goes beyond 9 GPa the difference in enthalpy between $BeSiO_3$ and the decomposition products becomes

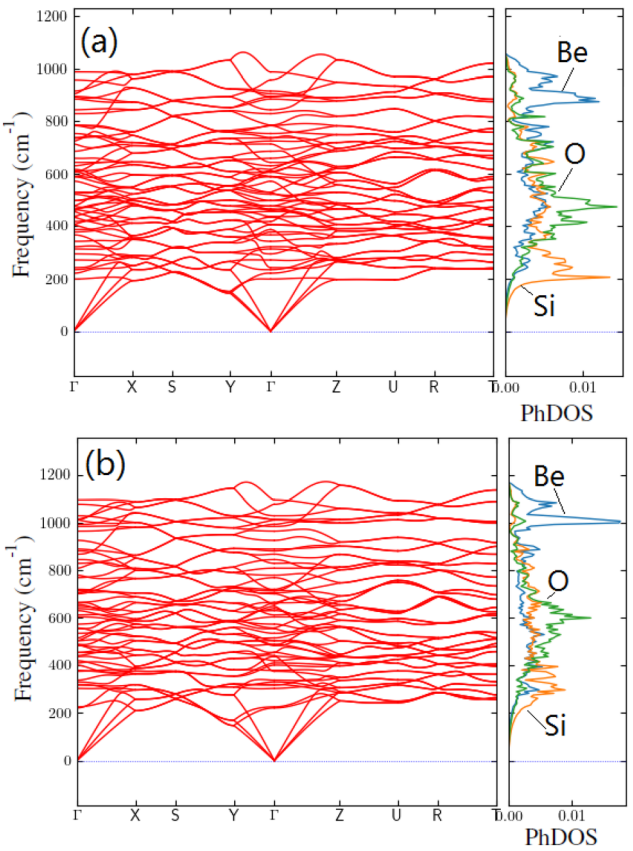

Fig. 4 Phonon dispersion and phonon density of states (PhDOs) calculated for orthorhombic $BeSiO_3$ at (a) 0 GPa and (b) 27 GPa.

more negative. This fact means that at these pressure conditions ($P < 9$ GPa), $BeSiO_3$ might probably be synthesized in a laboratory using a large-volume press and, due to the small enthalpy difference at 0 GPa between the orthorhombic structure and $(Be_2SiO_4 + SiO_2)/2$, $BeSiO_3$ might be recovered as a metastable phase after quenching at ambient conditions.[35] A pressure of 9 GPa corresponds to about 270 km in depth in the Earth's mantle. Thus, orthorhombic $BeSiO_3$ could exist in addition to phenakite Be_2SiO_4 in the interior of our planet. It should be here noted that calculations here are performed at 0 K, therefore the synthesis conditions might slightly differ for 9 GPa due to thermal effects or the influence of energy barriers. To estimate if the thermal effects may play a meaningful role in the transition pressure, we have also estimated the Gibbs free energy at 0 and 300 K. As expected for a solid–solid phase transition, thermal effects are negligible. When thermal contributions from Γ point phonons are considered, the difference between the Gibss energy and the enthalpy is ≈1 meV at 0 GPa and less than 4 meV at 10 GPa and 0 K, and ≈3 meV at 0 GPa and less than 0.2 meV at 10 GPa at 300 K. Although the estimation of kinetic energy barriers requires a different analysis, our thermodynamic results undoubtedly show that high pressure favors the stabilization of orthorhombic $BeSiO_3$. To complete this part of the discussion, we would like to stress that the synthesis of $BeSiO_3$ could be affected by the kinetic of

the process. If the kinetics are affected by energy barriers, then one can experimentally observe the coexistence of $BeSiO_3$, Be_2SiO_4, and BeO at pressures higher than the theoretically predicted transition pressure. In such a case, higher pressures than 9 GPa, or the combination of pressure and temperature, will be needed to synthesize $BeSiO_3$.

The orthorhombic structure of $BeSiO_3$ is represented in Fig. 1b. The lower symmetry of this structure, compared to the cubic structure, is associated with the tilting of the SiO_6 octahedral units, which gives rise to an orthorhombic structure with space group *Pnma*. In this structure, the unit cell contains four formula units ($Z = 4$) instead of one as in the cubic structure. The space groups of the cubic and orthorhombic structures are related *via* group–subgroup relationships. Using a group–subgroup transformation, it can be seen that if $\vec{a}$ of the orthorhombic structure is equal to $\vec{a} + \vec{c}$ of the cubic structure, $\vec{c}$ of the orthorhombic structure is equal to $\vec{a} - \vec{c}$ of the cubic structure, and $\vec{b}$ of the orthorhombic structure is equal to $2\vec{b}$ of the cubic structure, the orthorhombic structure and the cubic structure are equivalent. The extra flexibility provided by octahedral tilting and the changes in lattice parameters make the orthorhombic structure stable (while the cubic structure is not).

The calculated unit-cell parameters of the orthorhombic structure are shown in Table 1. The unit-cell volume of the orthorhombic structure 155.57 Å^3 (38.89 Å^3 per one formula unit) is 7.5% smaller than the volume of the cubic structure 42.05 Å^3. Notice that in the orthorhombic structure the *b*-axis is elongated, and the *c*-axis is compressed, while the *a*-axis is nearly not modified, in comparison to the ideal values obtained *via* the group–subgroup transformation ($a = c =$ 4.9177 Å and b = 6.9547 Å) which were the initial values used for the optimization of the orthorhombic structure. The optimized positions of the atoms are: Be at 4*c* (0.15649, 0.25, 0.47461), Si at 4*a* (0, 0, 0), O at 4*c* (0.48885, 0.25, 0.34372), and 8*d* (0.30216, 0.56857, 0.18240). The Si atoms are in octahedral coordination and Be atoms occupy the empty spaces formed by the corner-sharing framework made by SiO_6 octahedra. These units are distorted with two long Si–O distances aligned with the *b*-axis and four short Si–O distances; see Table 1. The average Si–O bond distance is 1.819 Å. The Be atoms are coordinated by the four nearest oxygen neighbors, forming BeO_4 distorted tetrahedral units, with an average bond distance of 1.642 Å. Detailed information about bond distances can be found in Table 1. The tetrahedral coordination of Be is a distinctive feature of orthorhombic perovskite-type $BeSiO_3$ and other beryllium metasilicates, as beryl.[5] In perovskite $ASiO_3$ silicates, usually the divalent A cation has a coordination number larger than that of silicon. The distinctive behavior of $BeSiO_3$ is related to the small Shannon radii of Be,[36] which up to now have been reported only forming compounds where Be is either four-fold or six-fold coordinated.[36] The BeO_4 tetrahedral units of $BeSiO_3$ are similar to those of Be_2SiO_4 where the average Be–O distance is 1.639;[37] *i.e.* very similar to the average Be–O distance in orthorhombic $BeSiO_3$, 1.642 Å. In contrast, the Si coordination polyhedra are different in both compounds; in $BeSiO_3$ Si atoms are six-fold coordinated, while in Be_2SiO_4 they are four-fold coordinated.

3.2. Effects of pressure on the crystal structure: equation of state and mechanical properties

From our calculations, we have determined the pressure dependence of the unit-cell parameters and volume of $BeSiO_3$. The results are presented in Fig. 5. In this figure, it can be seen that the compressibility of the studied compound is slightly anisotropic. The values of the linear compressibility of each axis are $\kappa_a = 1.29(3) \times 10^{-3}$ GPa^{-1}, $\kappa_b = 1.55(4) \times 10^{-3}$ GPa^{-1}, $\kappa_c = 1.32(3) \times 10^{-3}$ GPa^{-1}. The unit-cell parameter *b* is slightly more compressible than the other two parameters, which have a similar compressibility. The anisotropic response to pressure is related to the way the SiO_6 octahedra are connected in the crystal structure. The SiO_6 octahedron in $BeSiO_3$ is distorted in a way that the Si–O bond that is aligned nearly parallel to the *b*-axis is elongated compared with the other four Si–O bonds. Thus, this bond is more compressible than the other because longer bonds are more compressible than shorter bonds,[39] and consequently, the *b*-axis is the more compressible axes.

The pressure dependence of the volume can be described using a third-order Birch–Murnaghan equation of state (EOS).[40] In this equation, the fitting parameters are the volume at zero pressure V_0, the bulk modulus at zero pressure B_0, and its pressure derivative B_0', the values of the three para-

Table 1 Unit-cell parameters, volume at zero pressure (V_0), bulk modulus (B_0), and its pressure derivative (B_0') determined from this study for the orthorhombic phase of $BeSiO_3$. The calculated elastic constants C_{ij} at 0 GPa, and the bulk (*B*), shear (*G*), and Young (*E*) modulus derived from them are also reported. The subindex V, R, and H identify values obtained using the Voigt, Reuss, and Hill approximations, respectively

a (Å)	b (Å)	c (Å)	V_0 (Å^3)	B_0 (GPa)	B_0'	Si–O (Å)	Be–O (Å)
4.966	7.160	4.374	155.6	242.7	4.22	1.771 (×4) 1.917 ×2	1.599 (×2) 1.622, 1.747

C_{11}	C_{12}	C_{13}	C_{22}	C_{23}	C_{33}	C_{44}	C_{55}	C_{66}
483.7	97.8	165.8	408.6	170.9	473.0	181.2	217.9	157.0

B_V	B_R	B_H	E_V	E_R	E_H	G_V	G_R	G_H
248.2	244.7	246.5	421.7	410.2	415.9	173.3	168.0	170.6

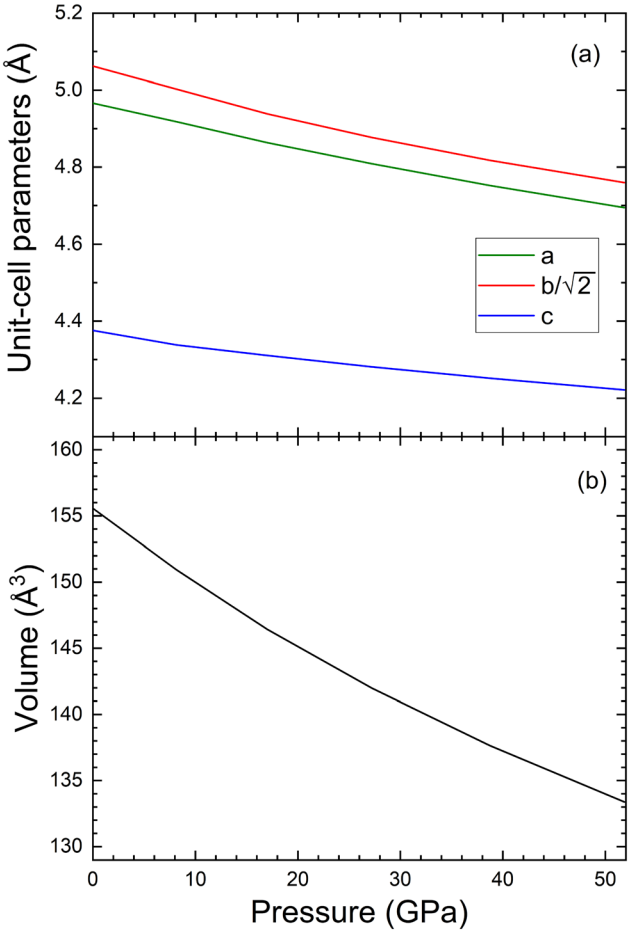

Fig. 5 Pressure dependence of (a) the unit-cell parameters and (b) the volume. The parameter *b* has been normalized to facilitate comparison.

meters determined from the fit are given in Table 1. The obtained bulk modulus, 242 GPa, is much larger than the same parameter in most silicates, including phenakite-type Be_2SiO_4 orthorhombic perovskite-type $CaSiO_3$, $MgSiO_3$ orthoenstatite, and olivine-type silicates, which have bulk moduli smaller than 220 GPa,[37,38,41] with the only exception of stishovite, B_0 = 297 GPa,[42] a dense tetragonal form of silicon dioxide, which is considered to be the predominant form in the lower mantle of Earth. The large bulk modulus of orthorhombic $BeSiO_3$ is consistent with the fact that it has a small unit-cell volume compared with other perovskite oxides and with the empirical law $K_0 \times V_0$ = constant followed by many oxides with the same structure.[43]

In order to assess the mechanical stability of $BeSiO_3$ and further understand its structural behavior under hydrostatic compression, we have calculated the elastic constants (C_{ij}). Their values at 0 GPa are given in Table 1, which also shows the bulk (B), shear (G), and Young (E) modulus obtained from C_{ij} using the Voigt,[44] Reuss,[45] and Hill[46] approximations. The elastic constants satisfy the Born criteria of stability for orthorhombic crystals,[47] indicating that orthorhombic $BeSiO_3$ is mechanically stable. Calculations of the elastic constants under high pressure support the mechanical stability of orthorhombic $BeSiO_3$ up to the highest pressure covered by our study. As it can be seen in Table 1, we found that ($C_{11} > C_{33} > C_{22}$), which is consistent with the sequence observed for the linear compressibilities $\kappa_b > \kappa_c > \kappa_a$. Regarding the bulk modulus, the three approximations give values of 244.7–248.2 GPa which are consistent with the value obtained from the pressure dependence of the volume, 242.7 GPa. On the other hand, the value of the Young modulus (410.2–421.7 GPa) is 75% larger than the bulk modulus, which indicates a large tensile (or compressive) stiffness of $BeSiO_3$ when a force is applied lengthwise. The value of the Young modulus of orthorhombic $BeSiO_3$ is also more than 50% larger than the same elastic modulus of silicates like $MgSiO_3$ orthoenstatite[48] and $CaSiO_3$ perovskite.[49] The large Young modulus of orthorhombic $BeSiO_3$ is connected to the fact that both BeO_4 tetrahedra and SiO_6 octahedra are very rigid units. In contrast in other $ASiO_3$ silicates the coordination polyhedra of the divalent cation A; *i.e.* Ca or Mg, are less rigid than BeO_4 tetrahedra. Notice that the differences in the bulk modulus between different $ASiO_3$ silicates and orthorhombic $BeSiO_3$ are not as large as differences in the Young modulus. This is because the volume changes related to the bulk modulus also involve changes in octahedral tilting. To conclude this part of the discussion we would like to comment on the shear modulus (G). Its value (168.0–173.2 GPa) indicates shear deformations are favored over volume and tensile contraction.

3.3. Bonding explanation of the mechanical properties

There is a common agreement that the bulk compressibility in ternary oxides can be expressed by means of cation oxide polyhedral compressibilities.[50,51] Following this criterion, here to explain the higher bulk modulus of $BeSiO_3$ compared to other silicate compounds, it is worth finding a polyhedral partition of the compressibility of the crystal. There are multiple partitions that can be done, however, we have decided to follow a chemical one generally used in the discussion of the silicates based on cationic polyhedra. To do such a partition, a special caution must be taken into account in this case. The volume of the unit cell can not be solely expressed as the sum of the volumes of the BeO_4 tetrahedra and SiO_6 octahedra, and therefore empty space needs to be taken into account. In this way, an exhaustive partition including the cation polyhedra that fill out the whole unit cell space could be expressed as:

$$V = 4V_{BeO_4} + 4V_{SiO_6} + V_{vac} \quad (2)$$

where V_{BeO_4}, V_{SiO_6}, and V_{vac} stand for the polyhedral building blocks in which the unit cell is divided. For instance, under zero pressure equilibrium conditions, the volume of the unit cell (155.57 Å^3; Z = 4) is divided into four tetrahedra with a total volume of 8.44 Å^3, four octahedra with a total volume of 31.76 Å^3, and the empty polyhedra occupying 115.40 Å^3.

The compressibility of the crystal (κ) can be expressed as the sum of the compressibility of each polyhedron occupied or not by cations (κ_i), multiplied by the occupation fraction that

Table 2 Polyhedral equations of state of $BeSiO_3$ according to our calculations

	f_i	B_i (GPa)	κ_i (GPa^{-1})
BeO_4	0.054	268.7	3.72×10^{-3}
SiO_6	0.204	246.4	4.06×10^{-3}
Empty	0.742	239.9	4.17×10^{-3}
Crystal	1.00	242.7	4.12×10^{-3}

each of them occupies (f_i) in the unit cell ($\kappa = \sum f_i \kappa_i$).[52] Table 2 shows the polyhedral contributions to the crystal compressibility. Taking into account the inverse relationship between compressibility and bulk modulus, we can evaluate B_0 of the crystal and compare it with the value obtained from the EOS fitting of the energy volume curve. An excellent agreement between the compressibility of the crystal and the bulk modulus is obtained from this decomposition. Differences between these two properties with respect to the value obtained from the crystalline EOS fitting are as low as 1.1×10^{-6} GPa^{-1} and 0.1 GPa, respectively. This supports the proposed polyhedral partition and the importance of including empty space.

According to our results, SiO_6 octahedra present a bulk modulus comparable to other silicates with Si atoms hexacoordinated to oxygen atoms as in the case of $CaSiO_3$ and SiO_2 stishovite.[42] On the other hand, the bulk modulus of BeO_4 tetrahedra is only 20 GPa higher than the value of SiO_6 despite occupying a fourth of the volume of the Si–O octahedra. The small difference between these two polyhedra can be explained in terms of the stronger covalent Si–O bond than Be–O bonds. The fact that BeO_4 units are also hard is what makes $BeSiO_3$ less compressible than related silicates.

The situation is more striking when we compare the bulk modulus of the empty space with the values of the cation polyhedra. Differences in the compressibility are as low as 3% and 12% compared to the SiO_6 and BeO_4, respectively. Indeed, as the volume of the empty space represents almost 75% of the unit cell, we would expect a greater compressibility for these regions according to the inverse volume–bulk modulus relationship.[28] These similar compressibilities are also evidenced by observing the relative variation of the polyhedral volumes in the pressure range studied, up to 52 GPa. The volume variation of the tetrahedron is about 0.24 $Å^3$, that of the octahedron is 0.30 $Å^3$, while that of the empty is only a little bit more, about 0.31 $Å^3$.

To further explore the underlying reasons for this *anomalous* behavior, we have analyzed how the electrons are distributed in the $BeSiO_3$ structure in comparison with its pure oxide counterparts (BeO and SiO_2) by means of the electron localization function (ELF) and QTAIM. BeO and SiO_2 crystals are characterized by highly polarized but also directional bonding situations and constitute good references for studying bonding in this silicate.[53–55] QTAIM characteristics are very similar in these three compounds. The Laplacian of the electron density at the Be–O and Si–O bonds critical points is positive, evidencing a closed shell interaction. Likewise, Bader charges reflect a high electron transfer between atoms. Be and Si are almost divalent and tetravalent cations (q_{Be} = 1.72 in BeO and $BeSiO_3$ and q_{Si} = 3.18 and 3.22 in SiO_2 and $BeSiO_3$) and O are dianions (q_O = −1.71, −1.61 and −1.63), respectively, as expected for these systems. Additionally, valence ELF attractor values in $BeSiO_3$ (see Table 3) are higher than 0.85 with populations around 2 electrons pointing to a strong electron localization around the oxygen cores as well as a high directionality towards the Be and Si atoms. Specifically, the ELF picture shows that Si atoms are described as bonded to six oxygen atoms in the expected octahedral coordination, whereas Be atoms are surrounded by four attractor centers connected to four oxygen atoms, building the BeO_4 units. This ELF picture and values are similar to the ones obtained in the BeO and SiO_2 crystals (see Table 4). In summary, the similarities in the ELF picture and QTAIM analysis on the Be–O and Si–O bonds, reinforce the idea that the Be–O and Si–O bonds in $BeSiO_3$ are highly polarized and directional, as occur in BeO and SiO_2. The directionality of the Be atoms in $BeSiO_3$ contrasts with the behavior of larger cations such as Ca in $CaSiO_3$, where the alkaline earth cation is located in the center of the voids left by the SiO_6 units. In the prototypical $CaSiO_3$, Ca atoms display a non-directional ionic interaction with twelve oxygen atoms in distorted cuboctahedral coordination.

As a result of the existence of BeO_4 units in $BeSiO_3$, two different types of oxygen atoms appear in contrast to the common $CaSiO_3$ crystal (see Fig. 6). One type of oxygen atom is coordinated with two Si atoms and two Be atoms. The ELF topological analysis evidences a tetrahedral environment

Table 3 ELF attractor (X) types, charges, volumes, distances to oxygen and cations and ELF attractor values (η_X) in orthorhombic $BeSiO_3$ at 0 GPa. Td, Oh and LP stand respectively for tetrahedral, octahedral, and lone pair attractors

X-type	d_{X-O} (Å)	d_{X-M} (Å)	Volume (a.u.)	n_{e^-} (e^-)	η_X
Td	0.71	0.92	29.69	2.30	0.889
Td	0.72	0.91	23.96	2.02	0.885
Td	0.66	1.12	18.77	1.98	0.873
Oh	0.70	1.07	14.41	1.49	0.865
Oh	0.71	1.08	15.50	1.51	0.862
Oh	0.77	1.29	19.30	1.76	0.855
LP(1)	0.59	—	14.04	1.39	0.858
LP(2)	0.60	—	18.46	1.59	0.857

Table 4 ELF attractor (X) types, charges, volumes, distances to oxygen and cations and ELF attractor values (η_X) in BeO and SiO_2 at 0 GPa. Td and LP stand respectively for tetrahedral and lone pair attractors

Structure	X-type	d_{X-O} (Å)	d_{X-M} (Å)	Volume (a.u.)	n_{e^-} (e^-)	η_X
SiO_2	Td	0.72	0.91	25.26	2.03	0.863
	Td	0.70	0.93	25.21	2.03	0.863
	LP	0.62	—	87.31	3.94	0.858
BeO	Td	0.72	0.92	24.22	1.99	0.880
	Td	0.69	0.96	20.02	2.00	0.879

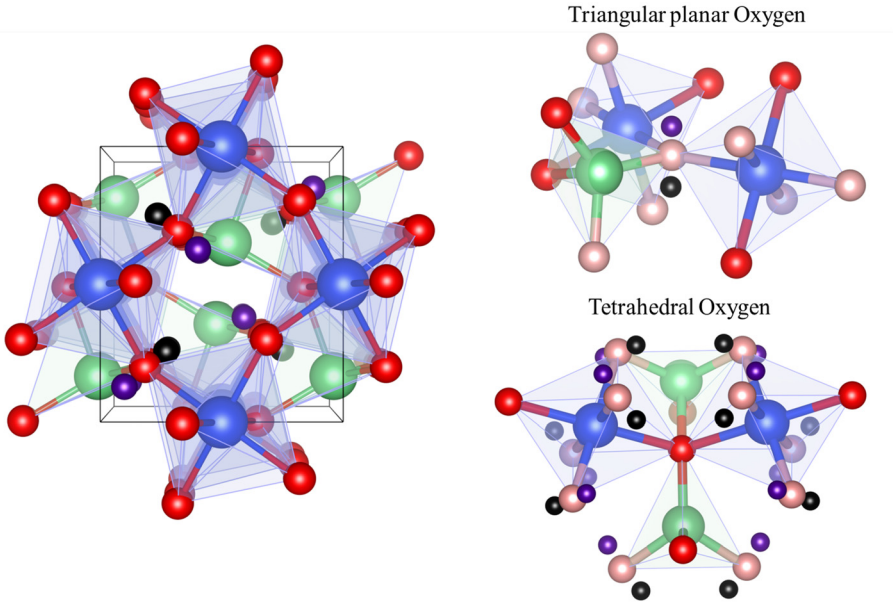

Fig. 6 Left panel: ELF lone-pair attractor centers (black and purple spheres) along the 100 plane in the $BeSiO_3$ structure. Right panel: Polyhedral fragments highlighting the environment of the triangular planar oxygen atoms coordinated to one Be and two Si atoms (pink) and the tetrahedrally coordinated to two Be and two Si atoms (red) along with their respective ELF lone-pair attractor centers. Blue and green spheres stand for Si and Be atoms, respectively.

without free lone-electron pairs for these oxygen atoms. The other type are those oxygen atoms connected to two Si and one Be atom in a triangular shape coordination. According to the ELF, these oxygen atoms formally display a non-bonded lone-electron pair distributed above and below the triangular plane and pointing towards the empty voids of the structure (see Fig. 6).

The directional character of the Be–O bonds and the concomitant non-bonded lone-electron pairs allow us to understand why the volume of the empty space of $BeSiO_3$ is not easily reduced as pressure is applied. The general compression mechanism of silicates implies either the rotation of their constitutive SiO polyhedra or the reduction of the interatomic distances. In our $BeSiO_3$ crystal, the rotation of the SiO_6 octahedra is hindered by the covalent nature of the Be–O bonds. Since edges are shared between SiO_6 and BeO_4 polyhedra, this rotation would strongly distort the BeO_4 tetrahedra producing a huge energy penalty. Analogously, the non-bonded lone-electron pairs are pointing toward the voids of the structure. Therefore, if SiO_6 octahedra rotates, a high repulsion between the different-faced lone-electron pairs in the empty void would be also created (see Fig. 6). Both situations make the empty space of the $BeSiO_3$ difficult to compress, making the reduction of the interatomic distances the only way to accommodate the pressure effects in this structure.

3.4. Phonon and electronic properties

We will now discuss the phonon spectrum of orthorhombic $BeSiO_3$. According to group-theory analysis, this compound has sixty vibrations with the following mechanical representation: $M = 7A_g + 8A_u + 5B_{1g} + 10B_{1u} + 7B_{2g} + 8B_{2u} + 5B_{3g} + 10B_{3u}$. One B_{1u}, one B_{2u}, and one B_{3u} are the acoustic modes. Among the optical modes, there are twenty-five infrared-active modes, $9B_{1u} + 7B_{2u} + 9B_{3u}$, twenty-four Raman-active modes, $7A_g + 5B_{1g} + 7B_{2g} + 5B_{3g}$, and eight silent modes, $8A_u$. The frequencies of all modes are summarized in Table 5 for 0 and 27 GPa. There, it can be seen that all modes harden under compression as a consequence of the decrease in the bond lengths. The modes with the smallest variation with pressure are the lowest frequency A_g Raman mode and the lowest frequency B_{2u} IR mode; see Table 5. Both modes are associated with vibrations of Si atoms. This fact can be clearly seen in the phonon dispersions calculated at 0 and 27 GPa which are shown in Fig. 4. The figure shows that all the modes below 300 cm^{-1} involve vibrations of Si atoms, the heaviest atom of the compound. On the other hand, modes from 300 to 800 cm^{-1} involve vibrations of O atoms; and modes above 800 cm^{-1} vibrations of Be atoms, the lightest atom of the compound.

To deepen the characterization of the studied material, we have finally calculated the electronic band structure and density of states. The results are represented in Fig. 7. We have found that orthorhombic $BeSiO_3$ is an insulator with a direct band gap at the Γ-point of the Brillouin zone which has a value of 7.15 eV at 0 GPa. In addition to the maximum of the valence band at Γ there is a second maximum close to it at the *Z* point. In the conduction band, there is a second minimum at the *Z* point which is 0.25 eV above the absolute minimum. We have also found that the top of the valence band is dominated by the O 2p orbitals, while the bottom of the conduction

Table 5 Calculated wavenumbers (ω) (in cm^{-1}) of Silent (S), Raman (R), and infrared (IR) modes of orthorhombic $BeSiO_3$ at 0 and 27 GPa

IR modes	ω at 0 GPa	ω at 27 GPa	R modes	ω at 0 GPa	ω at 27 GPa	S modes	ω at 0 GPa	ω at 27 GPa
B_{1u}	271.7	317.5	A_g	294.9	303.4	A_u	198.9	225.7
B_{1u}	405.9	420.1	A_g	342.9	379.3	A_u	234.6	320.1
B_{1u}	464.2	504.1	A_g	476.5	489.4	A_u	378.5	401.5
B_{1u}	521.5	572.7	A_g	588.9	638.4	A_u	434.9	455.3
B_{1u}	616.2	662.3	A_g	605.2	664.4	A_u	497.0	603.0
B_{1u}	658.6	713.0	A_g	610.9	704.7	A_u	630.1	719.2
B_{1u}	724.6	808.2	A_g	843.6	983.7	A_u	753.1	888.5
B_{1u}	785.0	925.2	B_{1g}	313.7	331.0	A_u	915.1	1013.6
B_{1u}	904.8	1011.0	B_{1g}	459.1	486.7			
B_{2u}	221.2	223.3	B_{1g}	497.4	611.5			
B_{2u}	242.6	375.6	B_{1g}	589.1	700.2			
B_{2u}	455.5	505.0	B_{1g}	987.5	1095.0			
B_{2u}	571.3	655.8	B_{2g}	407.9	441.8			
B_{2u}	643.1	715.5	B_{2g}	464.5	483.8			
B_{2u}	738.1	828.5	B_{2g}	529.1	556.6			
B_{2u}	894.7	1028.7	B_{2g}	588.5	629.9			
B_{3u}	322.5	338.4	B_{2g}	713.3	778.7			
B_{3u}	387.9	437.5	B_{2g}	828.9	963.9			
B_{3u}	418.7	454.8	B_{2g}	892.9	992.9			
B_{3u}	476.1	514.7	B_{3g}	367.7	410.7			
B_{3u}	528.9	554.0	B_{3g}	436.5	534.1			
B_{3u}	685.6	768.3	B_{3g}	607.3	647.5			
B_{3u}	734.9	844.3	B_{3g}	783.6	880.7			
B_{3u}	783.1	867.1	B_{3g}	884.7	1011.4			
B_{3u}	957.2	1076.7						

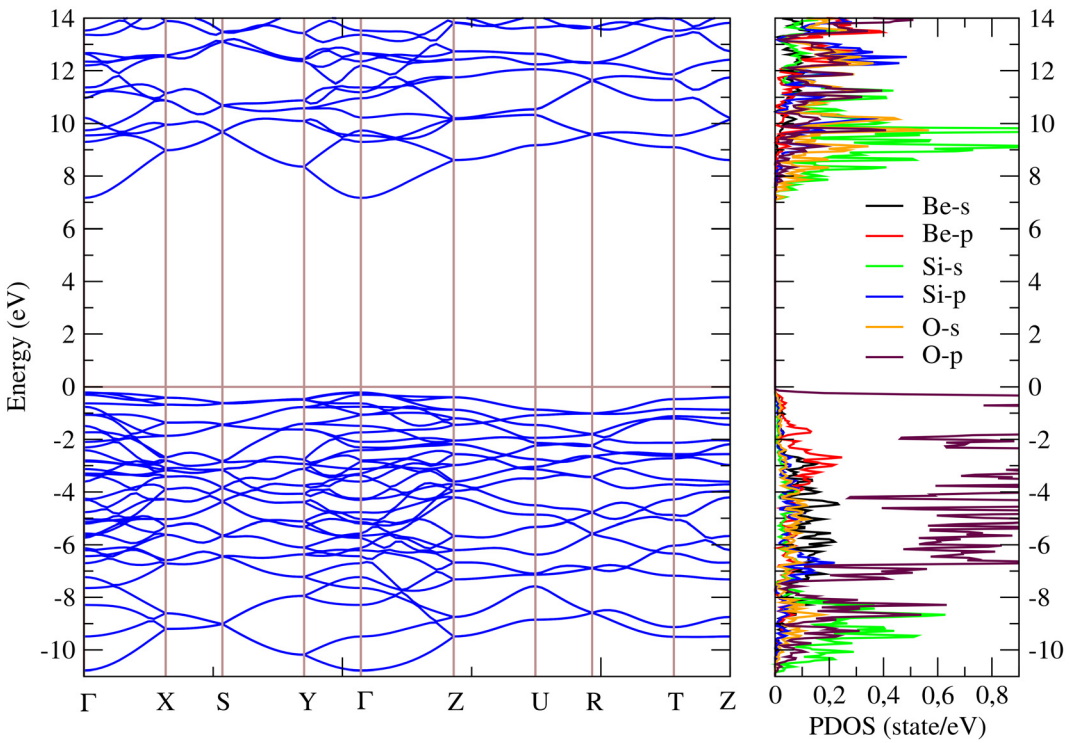

Fig. 7 Electronic band structure and partial electronic density of states (PDOS) of $BeSiO_3$ calculated at 0 GPa.

band is mainly contributed by Si 3p and O 2s states; see Fig. 7. Regarding the dispersion of the band structure, it can be seen that the conduction band is very dispersive and the valence band is nearly flat. In this regard, the topology of the band structure resembles that of the band structure of α-SiO_2.[56] This is because, in both compounds, the states near the Fermi level are contributed by the same orbitals of Si and O atoms. Interestingly, the minimum of the conduction band is parabolic. As pressure is increased, we have found that the band-gap energy increases up to 9.0 eV at 27 GPa. This is a conse-

quence of the enhancement of the repulsion between bonding and anti-bonding states due to the increase in crystal-filed splitting caused by the decrease of Si–O bond distances under compression.[57]

4. Conclusions

In this work, we have studied through density-functional theory simulations the possible formation of $BeSiO_3$ under high-pressure conditions, finding that this compound can be stabilized in an orthorhombic perovskite structure at pressures higher than 9 GPa and might probably be recovered as a metastable compound at ambient conditions. The crystal structure has been determined to be orthorhombic and described by space group *Pnma*. We have also found that this orthorhombic structure has a lower enthalpy than other typical structures of ABO_3 compounds, like hexagonal perovskite and Ilmenite-type, up to 50 GPa. The complete structural information of the orthorhombic structure has been reported, along with elastic, phonon, electronic, and bonding properties. The stability of the orthorhombic structure of $BeSiO_3$ is also supported by phonon-dispersion and elastic-constants calculations. The pressure dependence of unit-cell parameters has been reported, and the pressure-volume equation of state has been determined. $BeSiO_3$ is one of the less compressible silicates with a bulk modulus of 242 GPa. We have found that the high bulk modulus of the stable orthorhombic structure is closely related to the incompressible vacuum between the SiO_6 and BeO_4 polyhedra. Additionally, both the local bulk and the distortion of constituent polyhedra have been discussed in terms of the topological partition of the charge density and the bonding pattern. The results show that the edges shared between SiO_6 and BeO_4 polyhedra, and the vacuum space between them are also responsible for the strong distortion in the $BeSiO_3$ structure. We hope our computational study will motivate studies to experimentally obtain $BeSiO_3$ under high pressure.

Author contributions

T. O., R. F., A. L., F. I., A. M. investigation, formal analysis, writing review, and editing; D. E. Conceptualization, formal analysis, writing review and editing, and supervision.

Data availability

All relevant data are available from the corresponding author upon reasonable request.

Conflicts of interest

There are no conflicts to declare.

Acknowledgements

T. O. Thanks for the financial support given by PRFU under grant No. B00L02EP130220230001. R. F. acknowledges the financial support from Spanish MCIU and MINECO under projects MCIU-22-PID2021-122585NB-C21. D. E. and A. M. thank the financial support from Spanish Ministerio de Ciencia, Innovación y Universidades (MCIN, https://doi.org/10.13039/501100011033) under projects PID2022-138076NB-C41/44, and RED2022-134388-T and from Generalitat Valenciana (GVA) under grants PROMETEO CIPROM/2021/075 and MFA/2022/007. This study forms part of the Advanced Materials program and is supported by MCIN and GVA with funding from the European Union Next Generation EU (PRTR-C17.I1). The authors thank Professor Jos é Manuel Recio from the University of Oviedo for enlightening discussions.

References

1 T. Irifune, Absence of an aluminous phase in the upper part of the Earth's lower mantle, *Nature*, 1994, **370**, 131–133, DOI: 10.1038/370131a0.
2 R. M. Hazen and A. Y. Au, High-pressure crystal chemistry of phenakite (Be_2SiO_4) and bertrandite ($Be_4Si_2O_7(OH)_2$), *Phys. Chem. Miner.*, 1986, **13**, 69–78, DOI: 10.1007/BF00311896.
3 N. N. Greenwood and A. Earnshaw, *Chemistry of the Elements*, Butterworth-Heinemann, 2nd edn, 1997, ISBN 978-0-08-037941-8.
4 K. I. Machida, G. Y. Adachi, J. Shiokawa, M. Shimada and M. Koizumi, Structure and high-pressure polymorphism of strontium metasilicate, *Acta Crystallogr., Sect. B: Struct. Crystallogr. Cryst. Chem.*, 1982, **38**, 386–389, DOI: 10.1107/S0567740882003045.
5 B. Morosin, Structure and Thermal Expansion of Beryl, *Acta Crystallogr., Sect. B: Struct. Crystallogr. Cryst. Chem.*, 1972, **28**, 1899–1903, DOI: 10.1107/S0567740872005199.
6 https://www.chemicalbook.com/.
7 R. G. Parr, Density Functional Theory, *Annu. Rev. Phys. Chem.*, 1983, **34**, 631–656, DOI: 10.1146/annurev.pc.34.100183.003215.
8 T. Ouahrani, A. Muñoz, R. Franco, R. M. Boufatah, Z. Bedrane and D. Errandonea, High-pressure properties of thallium orthovanadate from density-functional theory calculations, *J. Alloys Compd.*, 2024, **978**, 173483, DOI: 10.1016/j.jallcom.2024.173483.
9 A. Benmakhlouf, D. Errandonea, M. Bouchenafa, S. Maabed, A. Bouhemadoud and A. Bentabet, New pressure-induced polymorphic transitions of anhydrous magnesium sulfate, *Dalton Trans.*, 2017, **46**, 5058–5068, DOI: 10.1039/C7DT00539C.
10 A. Jain, S. P. Ong, G. Hautier, W. Chen, W. D. Richards, S. Dacek, S. Cholia, D. Gunter, D. Skinner, G. Ceder and K. A. Persson, The Materials Project: A materials genome approach to accelerating materials innovation, *APL Mater.*, 2013, **1**, 011002, DOI: 10.1063/1.4812323.

11 https://legacy.materialsproject.org/materials/mp-1183445/.
12 K. Momma and F. Izumi, VESTA: a three-dimensional visualization system for electronic and structural analysis, *J. Appl. Crystallogr.*, 2008, **41**, 653–658, DOI: 10.1107/S0021889808012016.
13 J. P. S. Walsh and D. E. Freedman, High-Pressure Synthesis: A New Frontier in the Search for Next-Generation Intermetallic Compounds, *Acc. Chem. Res.*, 2018, **51**(6), 1315–1323, DOI: 10.1021/acs.accounts.8b00143.
14 D. E. Jung and A. R. Oganov, Ab initio study of the high-pressure behavior of $CaSiO_3$ perovskite, *Phys. Chem. Miner.*, 2005, **32**(2), 146–153, DOI: 10.1007/s00269-005-0453-z.
15 B. A. Wechsler and C. T. Prewitt, Crystal structure of ilmenite ($FeTiO_3$) at high temperature and high pressure, *Am. Mineral.*, 1984, **69**, 176–185, https://api.semanticscholar.org/CorpusID:46005030.
16 A. Labdelli and N. Hamdad, Perovskite oxides $MRuO_3$ (M=Sr, Ca and Ba): Structural distortion, electronic and magnetic properties with GGA and GGA-modified Becke–Johnson approaches, *Results Phys.*, 2015, **5**, 38–52, DOI: 10.1016/j.rinp.2014.10.004.
17 Y. Wang, Large Volume Presses for High-Pressure Studies Using Synchrotron Radiation, ed. E. Boldyreva and P. Dera, in *High-Pressure Crystallography. NATO Science for Peace and Security Series B: Physics and Biophysics*, Springer, Dordrecht, 2010. DOI: 10.1007/978-90-481-9258-88.
18 L. XiangChun, H. Rongzi and T. Changsheng, Tolerance factor and the stability discussion of ABO_3-type ilmenite, *J. Mater. Sci.: Mater. Electron.*, 2008, **20**(4), 323–327, DOI: 10.1007/s10854-008-9728-8.
19 V. M. Goldschmidt, Die Gesetze der Krystallochemie, *Naturwissenschaften*, 1926, **14**, 477–485, DOI: 10.1007/BF01507527.
20 G. Kresse and J. Furthmüller, Efficiency of ab initio total energy calculations for metals and semiconductors using a plane-wave basis set, *Comput. Mater. Sci.*, 1996, **6**, 15, DOI: 10.1016/0927-0256(96)00008-0.
21 G. Kresse and J. Hafner, Ab initio molecular dynamics for liquid metals, *Phys. Rev. B: Condens. Matter Mater. Phys.*, 1993, **47**, 558–561, DOI: 10.1103/PhysRevB.47.558.
22 P. E. Blochl, Projector augmented-wave method, *Phys. Rev. B: Condens. Matter Mater. Phys.*, 1994, **50**, 17953, DOI: 10.1103/PhysRevB.50.17953.
23 H. J. Monkhorst and J. D. Pack, Special points for Brillouin-zone integrations, *Phys. Rev. B: Solid State*, 1976, **13**, 5188, DOI: 10.1103/PhysRevB.13.5188.
24 J. P. Perdew, K. Burke and M. Ernzerhof, Generalized gradient approximation made simple, *Phys. Rev. Lett.*, 1996, **77**, 3865, DOI: 10.1103/physrevlett.77.3865.
25 J. Heyd, G. E. Scuseria and M. Ernzerhof, Hybrid functionals based on a screened Coulomb potential, *J. Chem. Phys.*, 2003, **118**, 8207–8215, DOI: 10.1063/1.1564060.
26 A. Togo and I. Tanaka, First principles phonon calculations in materials science, *Scr. Mater.*, 2015, **108**, 1–5, DOI: 10.1016/j.scriptamat.2015.07.021.
27 X. Gonze and C. Lee, Dynamical matrices, Born effective charges, dielectric permittivity tensors, and interatomic force constants from density-functional perturbation theory, *Phys. Rev. B: Condens. Matter Mater. Phys.*, 1997, **55**, 10355–10368, DOI: 10.1103/PhysRevB.55.10355.
28 T. Ouahrani, F.-Z. Medjdoub, S. Gueddida, Á. Lobato-Fernandez, R. Franco, N.-E. Benkhettou, M. Badawi, A. Liang, J. Gonzalez and D. Errandonea, Understanding the Pressure Effect on the Elastic, Electronic, Vibrational, and Bonding Properties of the $CeScO_3$ Perovskite, *J. Phys. Chem. C*, 2021, **125**(1), 107–119, DOI: 10.1021/acs.jpcc.0c08641.
29 A. Otero-de-la-Roza, M. A. Blanco, A. Martín Pendás and V. Luaña, Critic: a new program for the topological analysis of solid-state electron densities, *Comput. Phys. Commun.*, 2009, **180**, 157–166, DOI: 10.1016/j.cpc.2008.07.018.
30 S. Meziane, H. Feraoun, T. Ouahrani and C. Esling, Effects of Li and Na Intercalation on Electronic, Bonding, and Thermoelectric Transport Properties of MX_2 (M = Ta; X = S or Se) Dichalcogenides–Ab initio Investigation, *J. Alloys Compd.*, 2013, **581**, 731–740, DOI: 10.1016/j.jallcom.2013.07.033.
31 R. F. W. Bader, *Atoms in molecules*, Oxford University Press, Oxford, 1990.
32 S. Belarouci, T. Ouahrani, N. Benabdallah, A. Morales-García and I. Belabbas, Two-dimensional silicon carbide structure under uniaxial strains, electronic and bonding analysis, *Comput. Mater. Sci.*, 2018, **151**, 288–295, DOI: 10.1016/j.commatsci.2018.05.020.
33 S. Belarouci, T. Ouahrani, N. Benabdallah, A. Morales-García and R. Franco, Quantum-mechanical simulations of pressure effects on $MgIn_2S_4$ polymorphs, *Phase Transitions*, 2018, **91**, 759–771, DOI: 10.1080/01411594.2018.1480782.
34 T. Ouahrani, R. Khenata, B. Lasri, A. H. Reshak, A. Bouhemadou and S. Bin-Omran, First and second harmonic generation of the XAl_2Se_4 (X = Zn, Cd, Hg) defect chalcopyrite compounds, *Phys. B*, 2012, **407**(18), 3760–3766, DOI: 10.1016/j.physb.2012.05.057.
35 J. V. Badding, L. J. Parker and D. C. Nesting, High-Pressure Synthesis of Metastable Materials, *J. Solid State Chem.*, 1995, **117**, 229–235, DOI: 10.1006/jssc.1995.1268.
36 R. D. Shannon, Revised effective ionic radii and systematic studies of interatomic distances in halides and chalcogenides, *Acta Crystallogr., Sect. A: Cryst. Phys., Diffr., Theor. Gen. Crystallogr.*, 1976, **32**, 751–767, DOI: 10.1107/S0567739476001551.
37 J. Singh, D. Errandonea, V. Kanchana and G. Vaitheeswaran, Deep Earth Chronicles: High-Pressure Investigation of Phenakite Mineral Be_2SiO_4, *ChemPhysChem*, 2024, **25**, e202300901, DOI: 10.1002/cphc.202300901.
38 S. Ono, Elastic Properties of $CaSiO_3$ Perovskite from ab initio Molecular Dynamics, *Entropy*, 2013, **15**, 4300–4309, DOI: 10.3390/e15104300.
39 H. Yang, R. M. Hazen, L. W. Finger, C. T. Prewitt and R. T. Downs, Compressibility and crystal structure of silli-

manite, Al_2SiO_5, at high pressure, *Phys. Chem. Miner.*, 1997, **25**, 39–47, DOI: 10.1007/s002690050084.

40 F. Birch, Finite Elastic Strain of Cubic Crystals, *Phys. Rev.*, 1947, **71**, 809–824, DOI: 10.1103/PhysRev.71.809.

41 C.-C. Lin and C. Chien-Chih, Elasticity of tephroite (α-Mn_2SiO_4) and a comparison of the elastic properties of silicate olivines, *Eur. J. Mineral.*, 2011, **23**, 35–43, DOI: 10.1127/0935-1221/2011/0023-2077.

42 L.-G. Liu, Bulk moduli of SiO_2 polymorphs: Quartz, coesite and stishovite, *Mech. Mater.*, 1993, **14**, 283–290, DOI: 10.1016/0167-6636(93)90083-4.

43 R. M. Hazen and L. W. Finger, Bulk modulus-volume relationship for cation-anion polyhedra, *J. Geophys. Res.*, 1979, **84**, 6723–6728, DOI: 10.1029/JB084iB12p06723.

44 W. Voigt, Lehrbuch der Kristallphysik, Teubner Verlag, Leipzig, 1928, DOI: 10.1007/978-3-663-15884-4.

45 A. Reuss and Z. Angew, Berechnung der Fließlgrenze von Mischkristallen auf Grund der Plastizitätsbedingung für Einkristalle, *J. Appl. Math. Mech.*, 1929, **9**, 49, DOI: 10.1002/zamm.19290090104.

46 R. Hill, The Elastic Behaviour of a Crystalline Aggregate, *Proc. Phys. Soc., London, Sect. A*, 1952, **65**, 349, DOI: 10.1088/0370-1298/65/5/307.

47 G. Grimvall, B. Magyari-Köpe, V. Ozoliņš and K. A. Persson, Lattice instabilities in metallic elements, *Rev. Mod. Phys.*, 2012, **84**, 945–986, DOI: 10.1103/RevModPhys.84.945.

48 J. M. Jackson, S. V. Sinigeikin and J. D. Nass, Elasticity of $MgSiO_3$ orthoenstatite, *Am. Mineral.*, 1999, **84**, 677–680, DOI: 10.2138/am.2011.3632.

49 Z. J. Liu, X. W. Sun, Q. F. Chen, L. C. Cai, H. Y. Wu and S. H. Ge, First-principles study of the elastic and thermodynamic properties of $CaSiO_3$ perovskite, *J. Phys.: Condens. Matter*, 2007, **19**, 246103, DOI: 10.1088/0953-8984/19/24/246103.

50 J. M. Recio, R. Franco, A. Martín Pendás, M. A. Blanco, L. Pueyo and R. Pandey, Theoretical explanation of the uniform compressibility behavior observed in oxide spinels, *Phys. Rev. B: Condens. Matter Mater. Phys.*, 2001, **63**, 184101, DOI: 10.1103/PhysRevB.63.184101.

51 D. Errandonea, A. Muñoz, P. Rodr íguez-Hernández, O. Gomis, S. N. Achary, C. Popescu, S. J. Patwe and A. K. Tyagi, High-Pressure Crystal Structure, Lattice Vibrations, and Band Structure of $BiSbO_4$, *Inorg. Chem.*, 2016, **55**, 4958–4969, DOI: 10.1021/acs.inorgchem.6b00503.

52 T. Ouahrani, J. M. Menendez, M. Marqués, J. Contreras-García, V. G. Baonza and J. M. Recio, Local pressures in Zn chalcogenide polymorphs, *EPL*, 2012, **98**, 56002, DOI: 10.1209/0295-5075/98/56002.

53 T. Ouahrani, I. Merad-Boudia, H. Baltache, R. Khenata and Z. Bentalha, *Phys. Scr.*, 2011, **84**, 025704, DOI: 10.1088/0031-8949/84/02/025704.

54 M. A. Salvado, P. Pertierra, A. Morales-García, J. M. Menéndez and J. M. Recio, Understanding chemical changes across the α-cristobalite to stishovite transition path in silica, *J. Phys. Chem. C*, 2013, **117**, 8950–8958, DOI: 10.1021/jp800685u.

55 J. Contreras-García, A. Martín Pendás and J. M. Recio, How electron localization function quantifies and pictures chemical changes in a solid: The B3 → B1 pressure-induced phase transition in BeO, *J. Phys. Chem. B*, 2008, **112**, 9787–9794, DOI: 10.1021/jp800685u.

56 S. S. Nekrashevich and V. A. Gritsenko, Electronic Structure of Silicon Dioxide (A Review), *Phys. Solid State*, 2014, **56**, 207–222, DOI: 10.1134/S106378341402022X.

57 A. Liang, L.-T. Shi, R. Turnbull, F. J. Manjón, J. Ibáñez, C. Popescu, M. Jasmin, J. Singh, K. Venkatakrishnan, G. Vaitheeswaran and D. Errandonea, Pressure-induced band-gap energy increase in a metal iodate, *Phys. Rev. B*, 2022, **106**, 235203, DOI: 10.1103/PhysRevB.106.235203.